Video Article

# Visualizing Angiogenesis by Multiphoton Microscopy *In Vivo* in Genetically Modified 3D-PLGA/nHAp Scaffold for Calvarial Critical Bone Defect Repair

Jian Li[1], Holger Jahr[2,3], Wei Zheng[4], Pei-Gen Ren[1]

[1]Center for Translational Medicine Research and Development, Shenzhen Institutes of Advanced Technology, Chinese Academy of Sciences

[2]Department of Orthopedic Surgery, Maastricht UMC+

[3]Department of Orthopaedic Surgery, University Hospital RWTH

[4]Research Laboratory for Biomedical Optics and Molecular Imaging, Shenzhen Institutes of Advanced Technology, Chinese Academy of Sciences

Correspondence to: Wei Zheng at zhengwei@siat.ac.cn, Pei-Gen Ren at pg.ren@siat.ac.cn

URL: https://www.jove.com/video/55381
DOI: doi:10.3791/55381

Keywords: Bioengineering, Issue 127, bone defects, bone formation, 3D-PLGA/nHAp scaffold, genetically modified, angiogenesis, multiphoton microscopy

Date Published: 9/7/2017

Citation: Li, J., Jahr, H., Zheng, W., Ren, P.G. Visualizing Angiogenesis by Multiphoton Microscopy *In Vivo* in Genetically Modified 3D-PLGA/nHAp Scaffold for Calvarial Critical Bone Defect Repair. *J. Vis. Exp.* (127), e55381, doi:10.3791/55381 (2017).

## Abstract

The reconstruction of critically sized bone defects remains a serious clinical problem because of poor angiogenesis within tissue-engineered scaffolds during repair, which gives rise to a lack of sufficient blood supply and causes necrosis of the new tissues. Rapid vascularization is a vital prerequisite for new tissue survival and integration with existing host tissue. The *de novo* generation of vasculature in scaffolds is one of the most important steps in making bone regeneration more efficient, allowing repairing tissue to grow into a scaffold. To tackle this problem, the genetic modification of a biomaterial scaffold is used to accelerate angiogenesis and osteogenesis. However, visualizing and tracking *in vivo* blood vessel formation in real-time and in three-dimensional (3D) scaffolds or new bone tissue is still an obstacle for bone tissue engineering. Multiphoton microscopy (MPM) is a novel bio-imaging modality that can acquire volumetric data from biological structures in a high-resolution and minimally-invasive manner. The objective of this study was to visualize angiogenesis with multiphoton microscopy *in vivo* in a genetically modified 3D-PLGA/nHAp scaffold for calvarial critical bone defect repair. PLGA/nHAp scaffolds were functionalized for the sustained delivery of a growth factor *pdgf-b* gene carrying lentiviral vectors (LV-*pdgfb*) in order to facilitate angiogenesis and to enhance bone regeneration. In a scaffold-implanted calvarial critical bone defect mouse model, the blood vessel areas (BVAs) in PHp scaffolds were significantly higher than in PH scaffolds. Additionally, the expression of *pdgf-b* and angiogenesis-related genes, *vWF* and *VEGFR2*, increased correspondingly. MicroCT analysis indicated that the new bone formation in the PHp group dramatically improved compared to the other groups. To our knowledge, this is the first time multiphoton microscopy was used in bone tissue-engineering to investigate angiogenesis in a 3D bio-degradable scaffold *in vivo* and in real-time.

## Video Link

The video component of this article can be found at https://www.jove.com/video/55381/

## Introduction

Bone is a highly vascularized tissue that continues to remodel during the lifetime of an individual[1]. The rapid and effective bone regeneration of large bone defects resulting from trauma, nonunion, tumor resections, or craniofacial malformations is a complex physiological process. Traditional therapeutic approaches used for bone defect repair include autograft and allograft implantation, but their use involves several problems and limitations, such as limited availability, significant donor site morbidity, a high risk of infection, and host immune rejection[2,3]. However, artificial bone grafts offer an efficient alternative to alleviate these limitations. They can be made from biodegradable materials, are easy to be fabricate with a suitable pore size, and can be genetically modified[4,5].

Currently, various tissue engineering scaffolds have been employed in the development of tissue-engineered bone[6,7]. To induce bone repair and regeneration more effectively, engineered biomaterials combined with growth factors have emerged and achieved good results[8,9]. Unfortunately, the short half-life, easy-to-lose activity, and supraphysiological dosage of growth factors for therapeutic efficacy limit their clinical application[10]. To overcome these problems, the delivery of growth factor genes instead of growth factors has been demonstrated as an effective approach to sustain bioactivity for the treatment of osseous defects and diseases[11,12]. Viral vectors are promising delivery tools for tissue regeneration due to their high expressing efficiency[13].

Among growth factors, platelet-derived growth factor (PDGF-BB) was selected in this study because it is not only a mitogen and chemoattractant for mesenchymal and osteogenic cells, but also a stimulant for angiogenesis[14,15]. Previous preclinical and clinical studies showed that PDGF-BB could safely and effectively promote bone repair in periodontal osseous defects[16,17]. Recent studies revealed that PDGF-BB stimulates angiogenesis by motivating endothelial cell migration and proliferation *in vivo*[18,19]. Furthermore, PDGF-BB can also render mesenchymal stem cells (MSCs) capable of differentiating into endothelial cells[20], and this further highlights the potential role of MSCs in neovascularization.

 

Therefore, inducing the *de novo* formation of vasculature in scaffolds with PDGF-BB is an important step for the repair of tissue grown into scaffolds in bone tissue engineering.

Bone defect healing is a dynamic tissue morphogenetic process that requires coordinated osteogenesis and angiogenesis at the repairing positions[21]. Neoangiogenesis into implanted tissue-engineered scaffolds is an essential pre-requisite for supplying cells with nutrients and oxygen for growth and survival and for removing metabolic waste. Commonly used imaging methods, including X-ray micro-computed tomography (microCT), magnetic resonance imaging (MRI), scanning electron microscopy (SEM), optical coherence tomography (OCT), and confocal laser scanning microscopy, are applied instead of histological examination to obtain angiogenesis information[22,23]. However, these methods face various obstacles in visualizing and measuring neovasculature in 3D scaffolds in bone tissue engineering. Multiphoton microscopy (MPM) is a comparatively novel bio-imaging technique that has the distinct advantage of simultaneously visualizing cells, extracellular matrix, and surrounding vascular networks *in vivo*. It possesses an inherent three-dimensional imaging capability for deep tissue penetration and causes low photodamage. Hence, in the last decade, MPM has gained much attention in biomedical studies[24], including in neuroscience, immunology, and stem cell dynamics. However, it is barely used in orthopedic research.

## Protocol

The animal care was in compliance with the Guide for the Care and Use of Laboratory Animals of Guangdong Province. All procedures were performed under the supervision and approval of the Ethics Committee for Animal Research, Shenzhen Institutes of Advanced Technology, Chinese Academy of Sciences.

## 1. Lentiviral (LV) Production

1. Clone the *pdgf-b* cDNA into a lentiviral expression vector (pLenti6/5-eGFP or LV-eGFP) at a custom multiple-cloning site downstream of the cytomegalovirus promoter using Spe I and Sal I restriction sites to construct the pLenti6/5-PDGFB-eGFP plasmid (LV-*pdgfb*)[25].
2. Produce lentiviral particles (LV-*pdgfb*) from HEK-293FT cells by co-transfecting with virus packaging plasmids (pLP1, pLP2, and pVSV-G) using the standard calcium phosphate method with chloroquine (final concentration: 25 μM)[25].
3. After 48 h of transfection, harvest and filter 500 mL of virus-containing supernatant with a filter (0.45 μm). Subsequently, concentrate the viral particles by ultracentrifugation at 89,000 x g for 2 h. Resuspend in 200 μL of phosphate-buffered saline (PBS), aliquot, and store at -80 °C.
4. To determine the titer of lentivirus, incubate HEK293T cells with serially diluted lentiviral solution for 24 h and calculate the lentiviral titer, as previously described[25].

## 2. Fabrication of 3D-printed PLGA/nHAp Scaffolds and LV Immobilization

1. Dissolve 20 g of PLGA (Poly D,L-lactide-co-glycolide) material in 20 mL of 1,4-dioxane to form a homogeneous solution. Add 2 g of nanosized HAp (nano-hydroxyapatide) powder (nHAp) to the solution; the PLGA: nHAp ratio should be 10:1 (w/w).
2. Stir the mixed solution vigorously (stirring speed: 1,500 rpm) at room temperature for 16 h using a magnetic stirrer to form a uniform paste. Fabricate it into porous PLGA/nHAp scaffolds using a 3D low-temperature printer with a computerized nozzle that deposits the paste layer-by-layer, bottom to top, according to a predesigned model[26]; the pore sizes of the scaffolds range from 200 to 400 μm.
3. Vacuum freeze-dry the scaffolds for 48 h to remove solvent as completely as possible. Soak the scaffolds in 75% ethanol solution for 1 h for sterilization and lyophilize to get neutral, aseptic scaffolds.
   NOTE: The major parameters for vacuum freeze-drying include the condensation temperature (°C) and vacuum degree (Pa). Under a vacuum degree of 45 Pa, the PLGA/nHAp scaffolds were vacuum freeze-dried at -78 °C for 48 h to thoroughly remove the solvent.
4. Add 10 μL of LV particles ($4.5 \times 10^5$) to each PLGA/nHAp scaffold (4 mm x 4 mm x 2 mm) and incubate the scaffolds for 2 h at 37 °C in a humidified incubator to allow adsorption.
5. After immobilization, rinse the scaffolds twice with PBS to remove unbound LV particles. Snap-freeze the LV particle-coated scaffolds in liquid nitrogen, lyophilize again, and store at -80 °C for future use.

## 3. *In Vitro* Kinetics of LV Particle Release from Scaffolds and LV Transduction Activity Assay

1. Incubate 3D scaffolds (4 mm x 4 mm x 2 mm) carrying LV-green fluorescent protein (LV-eGFP, $4.5 \times 10^5$ LV particles) in 1 mL of complete DMEM in 2.0 mL cryogenic vials at 37 °C with shaking for 5 days.
2. Take a 1 mL sample every 12 h from 12 h to 120 h post-incubation and replace the medium. At each time point, add 1 mL of fresh medium instead of 1 mL of incubation medium.
3. **Use the collected media to transduce HEK293T cells by co-incubating for 48 h. Measure the number of bioactive LV particles by determining the number of GFP-positive HEK293T cells by flow cytometry[27].**
   1. Before transducing the HEK293T cells, remove the culture medium and rinse the HEK293T cells twice with PBS. Add the collected media containing lentivirus released from the scaffolds to the well (1 mL/well) and culture with the HEK293T cells for 48 h at 37 °C in a humidified incubator.

## 4. *In Vitro* Assessment of Bone Marrow-derived MSC (BMSC) Migration

1. Before the migration assay, prepare BMSCs expressing tomato fluorescent protein (BMSCs-T) and PDGF-BB protein (BMSCs-P)[28].
2. **Perform the BMSC migration assay with a Boyden chamber using a 24-well plate and polycarbonate filters with a pore size of 8 μm.**

1. Place 0.5 mL of BMSCs (5 x $10^4$) transfected with LV expressing tomato fluorescent protein (BMSCs-T) in the upper chambers. Place 0.5 mL of BMSCs (2 x $10^5$) transfected with LV expressing PDGF-BB protein (BMSCs-P) in the lower chambers.

3. Include six groups in this experiment and add 500 µL to the lower compartment of each well.
   A. Blank control, serum-free medium only
   B. FBS control, medium supplemented with 10% FBS
   C. PDGF-BB control, 4 ng/mL PDGF-BB in serum-free medium
   D. PDGF-BB seize group, PDGF-BB (4 ng/mL) and anti-PDGF-BB (4 ng/mL) polyclonal antibody in serum-free medium
   E. BMSC group, 2 x $10^5$ BMSCs in serum-free medium
   F. BMSCs-P group, 2 x $10^5$ BMSCs-P in serum free medium.
4. **Incubate for 48 h at 5% $CO_2$ and 37 °C in a humidified incubator. Afterwards, remove the migrated cells on the lower chamber side and collect them for quantification of the number of BMSCs-T by flow cytometry.**
   1. Remove migrated cells on the lower chamber side using a cell scraper and resuspend the migrated cells with 2 mL of PBS. Quantify the number of migrated BMSCs-T by flow cytometry[29].

## 5. Establishment of a Murine Calvarial Critical Bone Defect Model and Scaffold Transplantation

NOTE: Male BALB/c mice (7 weeks old) were purchased from Guangdong Medical Laboratory Animal Center (Guangdong, China).

1. Enroll a total of 42 male mice for the calvarial bone defect experiment. Randomly divide the mice into three groups, with fourteen in each group that receive the following treatments: Group A, no implants; Group B, PH scaffolds implanted (PLGA/nHAp); and Group C, PHp scaffolds implanted (PLGA/nHAp/LV-*pdgfb*).
2. Anesthetize the animals with the intraperitoneal administration of sodium pentobarbital (50 mg/kg). Remove fur with depilatory paste and clean the head skin with 75% alcohol solution before making the first incision. Fix the head of each mouse with a stereotactic instrument to keep it still during surgery.
3. Make an initial incision with a scalpel and then enlarge it with scissors to create a 1-cm linear skin incision. Scrape the periosteum from the bone of the cranium to reveal the bone surface of the skull using a sterile cotton swab.
4. Use a trephine burr to create a 4 mm-diameter critical-size defect on the left side of the calvaria[30]. Transplant the scaffold into the bone defect site.
   NOTE: Critical size defects (CSDs) were originally defined as "the smallest size intraosseous wound in a particular bone and species of animal that will not heal spontaneously during the lifetime of the animal." In this experiment, the 4 mm-diameter defect is a critical size bone defect, according to the previously study[31,32].
5. Use ophthalmic forceps to move the periosteum back gently to cover the surgical site. Suture the incised skin with three stitches per cm.
6. Perform post-operational care. Administer the analgesic buprenorphine (0.1 mg/kg) to relieve pain. Maintain the body temperature with a heating pad until the animal awakens. Subsequently, feed the animals with food and water and record their activity every day until the end of the test. Note: Analgesia can be administered prior to the procedure depending on your local animal care committee guidelines.

## 6. *In Vivo* Imaging of Angiogenesis Within the Bone Defect with MPM

NOTE: FITC-conjugated 250 kD dextran (10 mg/mL) in saline was intravenously injected into mice to obtain high-SNR (signal-to-noise ratio) images of new blood vessels according to a previous study[33]. Please note that this is a survival procedure.

1. Assemble the multiphoton microscopy (MPM) system for two-photon excited fluorescence (TPEF) and second harmonic generation signal (SHG) imaging.
2. Anaesthetize the animals with an intraperitoneal injection of pentobarbital sodium (50 mg/kg) and immobilize the animals on a heating plate to maintain their body temperature at 37 °C throughout the experiments. Use 3.0% isoflurane gas in 100% oxygen to maintain satisfactory anesthesia and analgesia during the imaging process. Intraperitoneally inject saline (200 µL/animal) to prevent dehydration before imaging.
3. Tune the femtosecond Ti-Sapphire laser to 860 nm. Create a 512 x 512 µm sampling area by scanning a pair of galvo mirrors and use NA1.0 water-immersion objective lens to focusthe excitation beam into the sample and to collect the backscattered TPEF/SHG signal.
   NOTE: The imaging was performed on a home-build multiphoton microscopic imaging system (MPM). During imaging, a femtosecond Ti-Sapphire laser was tuned to 860 nm as the optimal excitation wavelength. The laser beam was raster scanned across a sample plane using a pair of galvanometer mirrors. After passing through a dichroic mirror of 685 nm, the beam was focused on the specimen by a 20X NA1.0 objective. The induced TPEF and SHG signals were collected by the same objective. The signals were split from the excitation laser by the dichroic mirror mentioned above and purified by a 680-nm short-pass filter. The TPEF and SHG signals were collected by a fiber bundle and conducted to a spectrograph. The detector on the spectrograph was a linear array of photomultiplier tubes (PMTs). The combination of spectrograph and linear array PMTs offered the capability to record the signal in 16 consecutive spectral bands, from 400 nm to 600 nm, at 12.5-nm intervals. Therefore, the TPEF and SHG signals were detected at the same time and separated in spectral domains. Furthermore, for 3D imaging, an axial motor was used to control the imaging depth. The area of each image was set to 512 x 512 µm, and the depth interval was set to 2 µm (control group, 5 µm). Notably, 5 sites on each defect were imaged to collect statistically significant data, and the selected imaging sites were distributed evenly and randomly along the defect.
4. **Scan 5 sites on each defect to collect statistically significant data to measure vessel formation.**
   1. Use scanning sites evenly and randomly distributed along the defect. For the control group, have the field of view (FOV) cover both the original bone area and the edge of the defect, but for the PH and PHp groups, have the FOV on the implanted scaffold.
   2. Make a 1-cm linear skin incision using a scalpel and suture the open skin to the fixation to reveal the transplantation site. Use a syringe to place a drop of water between the dipping lens and transplants to form a water glass.

5. Acquire image stacks every 12 s over a 2 h imaging period. Display and analyze volumetric data using a custom MATLAB program and quantify the blood vessel areas with ImageJ software[34,35].

## 7. Gene Expression Analysis of *pdgf-b* and Angiogenesis-related Genes by RT-qPCR

NOTE: PCR was performed following the usual steps: 95 °C for 30 s, 40 cycles of 95 °C for 5 s, and 60 °C for 30 s. Post-PCR melting curves confirmed the specificity of single-target amplification, and the fold change of the gene of interest relative to β-actin was determined. The reaction for each sample was tested three times.

1. Harvest implanted scaffolds and tissues from the experimental mice at 2, 4, and 8 weeks post-operation[36]; control group samples (n = 4), taken at the same time points, should be from adjacent bone tissue.
   NOTE: At each time point (2, 4, and 8 weeks), euthanized the mice with $CO_2$ inhalation. Dissect the calvaria and, subsequently, remove and harvest the implanted scaffolds from the calvaria.
2. Use a commercial reagent to extract the total RNA from each sample according to the manufacturer's protocol. Use the Reverse Transcription Kit to reverse-transcribe the RNA into cDNA following the manufacturer's protocol.
3. Perform quantitative real-time PCR using the SYBR Green Detection System; the primers are listed in **Table 1**.

| Primer(5'–3') | | |
|---|---|---|
| Gene | Forward | Reverse |
| pdgfb | CATCCGCTCCTTTGATGATCTT | GTGCTCGGGTCATGTTCAAGT |
| vWF | CTCTTTGGGGACGACTTCATC | TCCCGAGAATGGAGAAGGAAC |
| VEGFR2 | GAAATGACACTGGAGCCTACA AG | TCCATGCTGGTCACTAACAGAA G |
| β-actin | GTATCCATGAAATAAGTGGTTAC AGG | GCAGTACATAATTTACACAGAAG CAAT |

**Table 1: Pimer Sets.**

## 8. MicroCT Analysis of Bone Regeneration

1. Euthanize mice with $CO_2$ inhalation at 8 weeks post-operation. In a well-ventilated environment, gently place each mouse into a clean mouse cage and pump $CO_2$ gas into the cage to anaesthetize the mice before the euthanasia.
2. Dissect the skull for microCT imaging of the bone defect region. User the following scanning parameters in the experiments: 9 μm resolution, Al 0.5 mm filter, 50 kV voltage, and 142 μA current.
3. Reconstruct all imaging data using commercial software provided by the company. Calibrate the scans using the calibration function of a CTAn software.
   NOTE: Place a Hounsfield unit (HU) under the mice in each scan.

## Representative Results

Cylindrical Porous PLGA/nHAp scaffolds 0.6 mm in height and 4 mm in diameter were fabricated with a 3D printer. The morphologies of the scaffolds were analyzed via scanning electron microscopy and microCT. **Figure 1A** shows the photograph of the implanted scaffold. MicroCT scanning revealed that more than 85% of the pores had sizes ranging from 200 to 400 μm (**Figure 1B**). SEM imaging demonstrated that the surface of the scaffold had a rough microtopography, with micropores (diameters approximately 5 - 10 μm) that interconnected inside the scaffolds (**Figure 1D-F**). Approximately 40% of the total amount of coated LV-eGFP particles ($4.5 \times 10^5$) released from the PLGA/nHAp scaffolds started with an initial burst effect within 24 h. The bioactivity of released LV viruses reached summit at 24 h and then continuously diminished, approaching to 0 at 120 h (**Figure 2**). These data indicate that the bioactivity of most scaffold-immobilized LV particles could be maintained for up to 96 h. The migration capacity of MSCs-T was observed with the FACS method to investigate whether LV carrying *pdgf-b* cDNA could express and lead to BMSC chemotaxis, as shown in **Figure 3.** Both the positive control (**C**) and the PDGF-BB-expressing group (**F**) exhibited a significantly higher level of BMSC migration than the other 4 groups. In addition, the migration of BMSCs in Group F was significantly higher than that in Group C. There were no significant differences in BMSC migration among the other 4 groups.

Angiogenesis within the bone defect was assessed from the 2nd to the 8th week post-implantation by MPM scanning. **Figure 4A** shows a schematic illustration of a mouse under MPM scanning. Obvious angiogenesis was detected in the PH and PHp groups, but blood vessels were barely observable in the control group, where only a layer of fibrous membranes across the defect region formed (**Figure 4B**). The GIF graphs show the blood vessel tomographs of each group (**Supplementary Data**). The area of new blood vessels gradually increased over time in groups PH and PHp, with similar increasing patterns. At the 8th week, the vessels appeared similar in morphology to those observed at the early stage; the only change was that an increasing number of smaller vessels was growing into scaffolds (**Figure 4B**). The BVA of the PHp group was significantly higher than that of the other two groups at all time points (**Figure 4C**). Furthermore, there were many collagen deposition sites, as indicated by SHG signals (the green color in the graphs and GIF graphs) in the PH and PHp groups, but not in the control group (**Figure 4B**).

In order to clarify the relationship of PDGF-BB expression and angiogenesis, we compared the gene transcript expression levels of *pdgf-b*, *vWF*, and *VEGFR2* with the RT-qPCR method at 2, 4, and 8 weeks post-implantation (**Figure 5**). As expected, *pdgf-b* expression was significantly increased in the PHp group at all time points, with a 5- to 13-times increase compared to the control and PH groups (**Figure 5A**). There was no significant difference between the control and PH group, and the expression level of PDGF-BB almost remained constant from week 2 to week 8, as shown in **Figure 5A**. The mRNA expression levels of *vWF* and *VEGFR2* in all three groups gradually increased and were the highest in the PHp group at all three time points (**Figure 5B** and **5C**). For the PH group, there was no statistical significance compared to the control group, despite obvious angiogenesis (**Figure 4B**).

To further confirm that *pdgf-b*-containing scaffolds promote bone regeneration *in vivo* using critically sized calvarial defects in male BALB/c mice, microCT scanning supplied information to assess bone regeneration at 8 weeks post-implantation. As shown in **Figure 6**, defects in the PHp group were filled with a mass of new bone tissue ingrowth in the scaffolds, whereas there was much less new bone in the control and PH groups.

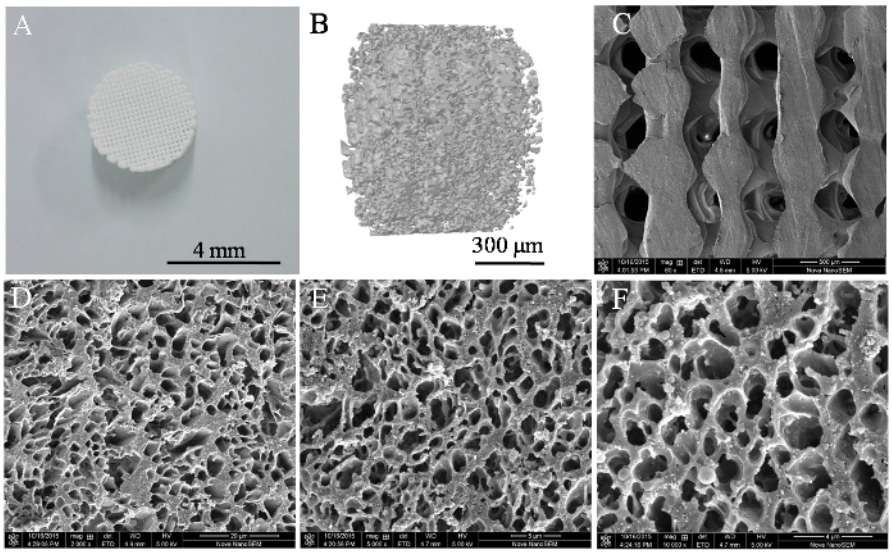


**Figure 1: Structural Characterization of a 3D PLGA/nHAp Scaffold.** (**A**) Photograph of a 3D printed scaffold. (**B**) A microCT image of the overall porosity of the scaffold. (**C**) The microtopography of the scaffold surface observed by SEM at 60X, 2,000X (**D**), 5,000X (**E**), and 10,000X magnification (**F**). Please click here to view a larger version of this figure.

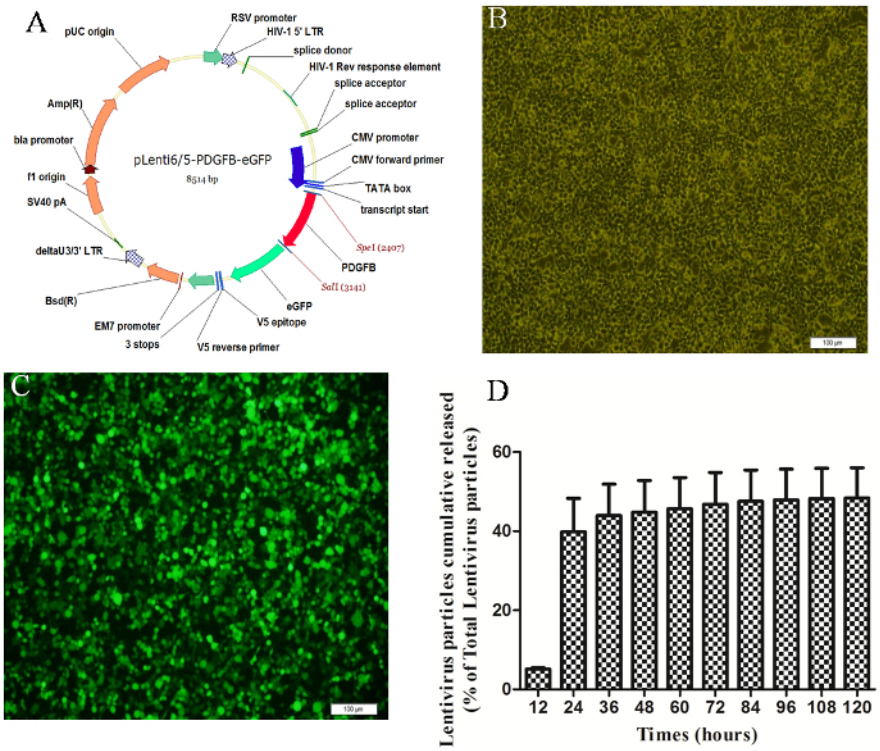


**Figure 2: Preparation of the Lentivirus and Evaluation of the Bioactivity of the LV-GFP Particles.** (**A**) Schematic representation of the lentiviral vector construct. After 48 h of transfection, HEK-293FT cells were observed under light (**B**) and fluorescence field (**C**) conditions. (**D**) *In vitro* assessment of the bioactivity of the LV-GFP particles cumulatively released from PLGA/nHAp scaffolds. All data are presented as the mean ± SEM (n = 4). Please click here to view a larger version of this figure.

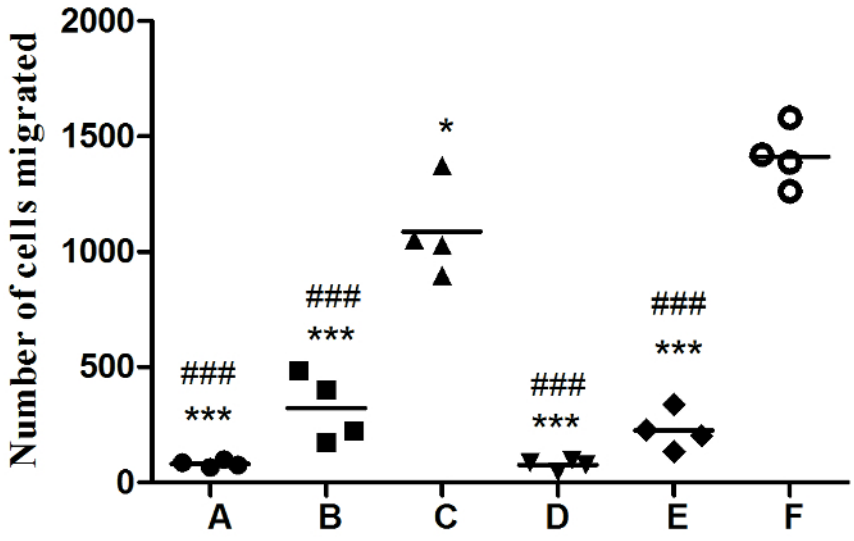


**Figure 3. PDGF-BB Bioactivity as a Potent Chemotactic Factor Response of BMSC Migration.** BMSCs-T (5 x $10^4$) were seeded on top of transwell chambers, with various condition media placed in the bottom of the chambers. (**A**) Blank control, serum-free medium only; (**B**) FBS control, medium supplemented with 10% FBS; (C) PDGF-BB control, 4 ng/mL PDGF-BB in serum-free medium; (**D**) PDGF-BB seize group, PDGF-BB (4 ng/mL) and anti-PDGF-BB (4 ng/mL) polyclonal antibody in serum-free medium; (**E**) BMSCs group, 2 x $10^5$ BMSCs in serum-free medium; and (**F**) BMSCs-P group, 2 x $10^5$ BMSCs-P in serum-free medium. All data are shown as the mean ± SEM (n = 4). #: comparison between group C and all other groups, except group F, $^{###}$ p <0.0001. *: comparison between group F and all other groups, * p <0.05, *** p <0.0001. Please click here to view a larger version of this figure.

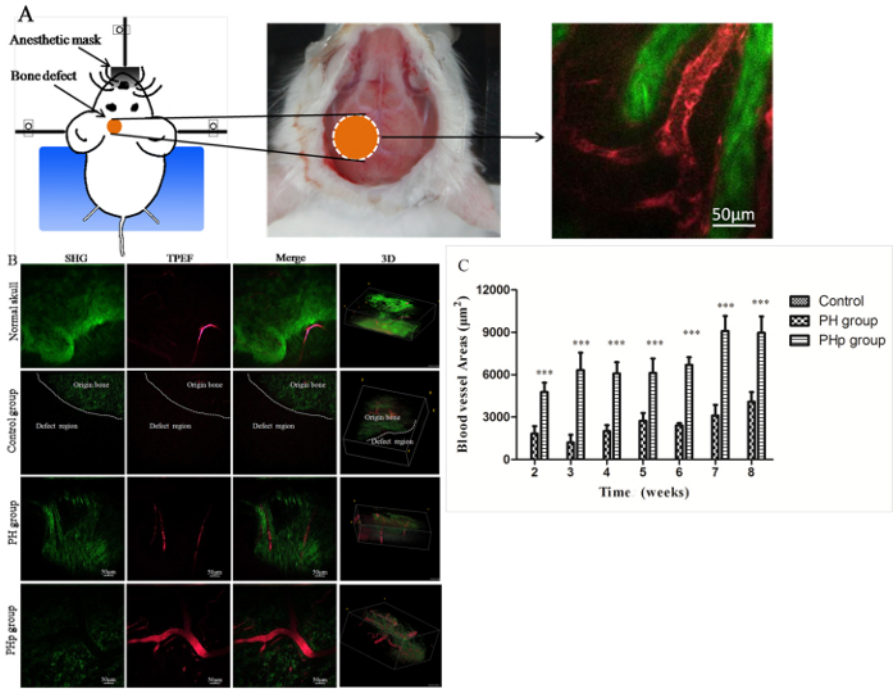


**Figure 4: High-resolution Multiphoton Microscopy (SHG/TPEF) Imaging and Quantification of Angiogenesis in the Bone Defect Region of Mouse Calvaria.** (**A**) A schematic illustration of a mouse under MPM scanning. The orange circle represents the defect site, the red tubules represent blood vessels, and the green represents collagen. (**B**) Unoperated and operated animals were scanned with MPM at 8 weeks post-implantation. SHG, TPEF, SHG/TPEF merged, and 3D images are shown. The dotted line represents the boundary along the bone defect in the control group based on SHG signals. (**C**) Blood vessel area quantification within the defect area of control, PH, and PHp from week 2 to week 8 post-implantation. All data are shown as the mean ± SEM (n = 5). ***: Statistical analysis between groups PH and PHp, p <0.0001. Please click here to view a larger version of this figure.

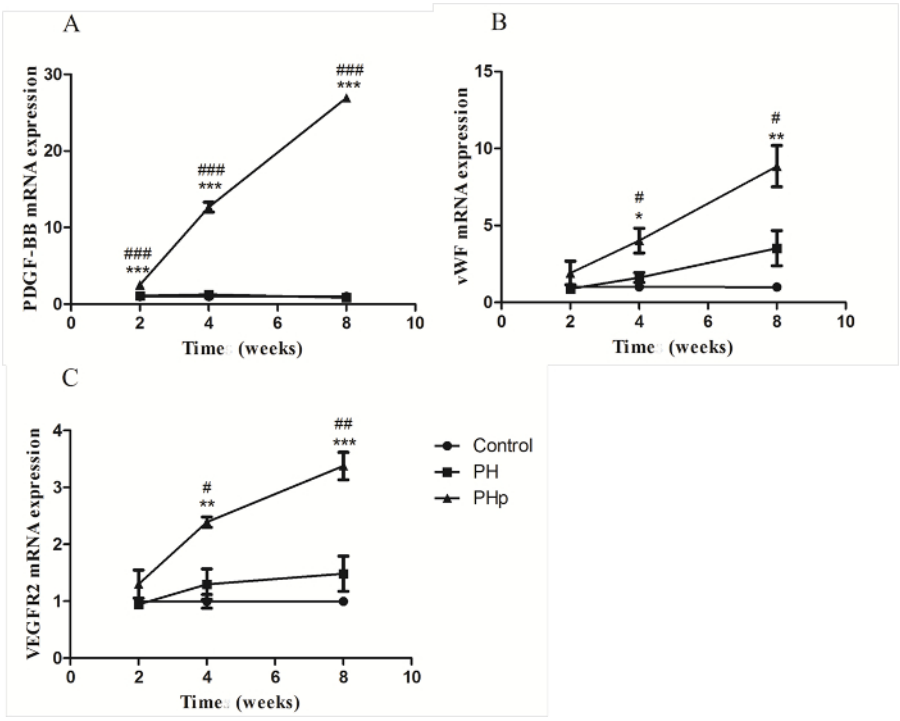


**Figure 5:** RT-qPCR Analysis of *pdgf-b* (**A**) and Angiogenesis-related Genes *vWF* (**B**) and *VEGRF2* (**C**) Expression in Three Groups. Samples from 4 animals were analyzed for each time point. #: comparison between the PHp and PH groups, $^{\#}$p <0.05, $^{\#\#}$p <0.01, and $^{\#\#\#}$p <0.0001. *: comparison between the PHp and control groups, *p <0.05, **p <0.01, and ***p <0.0001. Please click here to view a larger version of this figure.

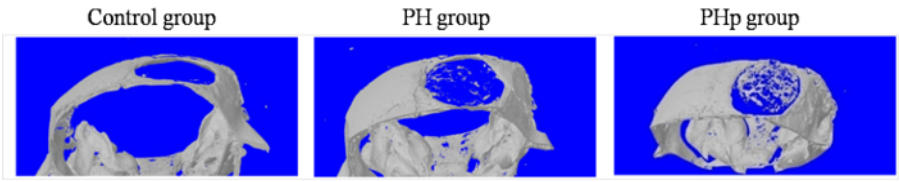


**Figure 6: Evaluation of *In Vivo* Bone Formation with MicroCT Scanning.** Control group without implanted scaffolds. PH group within implanted PLGA/nHAp scaffold only. PHp group within implanted PLGA/nHAp scaffold modified by the LV-*pdgfb* particles. Please click here to view a larger version of this figure.

## Discussion

Bone is a highly vascularized tissue with a unique capacity to continuously heal and remodel throughout the lifetime of an individual[1]. The level of vascularization is important for osteogenesis and defect repair. Low vascularization limits the wide clinical application of tissue-engineered bone. Constructing a highly vascularized tissue-engineered bone according to the theory of biomimetics has become a tool for repairing large segment bone defects. Various kinds of scaffolds have been successfully applied to repair comparatively small osseous defects. However, for critical bone defects, the application of scaffolds to repair still faces obstacles, mainly due to insufficient blood supply for defect repair. Therefore, improving the blood supply during the process of repairing large bone defects is one of the major issues in tissue engineering.

People use bioactive material-coated scaffolds to help to establish the necessary morphogenetic fields that can stimulate, recruit, and promote the chemotaxis, differentiation, and proliferation of the cells needed for neovasculature and bone formation[37]. Neovasculature in tissue-engineered scaffolds is essential for the cells to receive oxygen and nutrients, for the removal of waste products, and ultimately for the fulfillment of the function of scaffolds. The objectives of this study were to investigate angiogenesis with *in vivo* multiphoton microscopy in a genetically modified, 3D-printed PLGA/nHAp scaffold for calvarial critical bone defect repair and to evaluate the effects of bone regeneration using microCT.

Despite dramatic achievements in bone tissue engineering, the *in vivo* visualization and quantification of neovascularization in scaffolds during bone regeneration is still a challenge. Most microscopic imaging systems are unable to provide volumetric information on angiogenesis. Traditional imaging methods, such as microCT, MRI, and histological analyses, are destructive, complicated, and laborious and have low spatial resolutions and long image acquisition times[38]. However, MPM imaging is a novel bio-imaging modality that can capture blood vessel signals *in vivo* in a high-resolution and minimally invasive manner. It is able to detect new vessels thinner than 10 μm (**Figure 4B**). Besides blood vessel images, we also observed a mass of new collagen deposition (the green color in Figure 4B and the GIF graphs in the supplementary material), as indicated by SHG signals, which indicate bone tissue formation from another angle. Theoretically, blood vessel images could be obtained without the using of contrast agents. However, in the present study, we used a contrast agent to get better images and removed local skin to ensure the proper scanning depth. This would be unnecessary when more powerful imaging systems are available in the future for truly non-invasive imaging.

HAp is a biomedical material for bone tissue regeneration that is widely used due to its good osteoconduction and osteoinduction traits. HAp has good capability of binding DNA vectors and retaining and stabilizing vectors, including viral vectors[39]. Compared to microsized HAp, nanosized HAp particles possess high specific surface areas and therefore show better cellular behavior and mechanical properties[40]. For these reasons, nHAp particles are one of the components of the scaffolds. The surface and cross-sectional SEM images of the PLGA/nHAp scaffold shown in Figure 1 indicates that the fabricated scaffolds exhibit a well-interconnected pore structure and uniformly distributed pore sizes. The immobilization of virus onto biomaterial carriers can influence virus activity. Therefore, we tested the bioactivity of LV particles released from the scaffolds by investigating their transfection activity. The release profiles of LV particles from the scaffolds and their bioactivities were evaluated *in vitro*, demonstrating the controlled delivery of bioactive LV particles for five days (**Figure 2**). Furthermore, our *in vitro* study focused on the potential of PDGF-BB to stimulate the migration of primary MSCs. These results suggest that the LV particles expressed bioactive PDGF-BB and effectively stimulated BMSC migration.

To confirm the capacity for angiogenesis and bone regeneration *in vivo*, PHp scaffolds were implanted into murine calvarial critical bone defects. Vessel formation was confirmed with angiogenic markers, RT-qPCR analysis, and blood vessel densities observed with SHG/TPEF imaging. Both of the two sets of experiments demonstrated that angiogenesis and blood vessel formation were improved significantly with the treatment of genetically modified scaffolds. These results indicate that PDGF-BB not only directly stimulates angiogenesis, but also induces other angiogenesis-related genes. Meanwhile, microCT measurements demonstrate that *pdgf-b*-containing scaffolds significantly promoted bone formation compared to the unmodified scaffolds, which correlates well with the neovasculature in the scaffold. These results indicate that genetically modified, bioactive scaffolds significantly improve angiogenesis and tissue regeneration.

The results presented here demonstrate that the lentivirus-mediated genetic modification of scaffolds facilitates large osseous defect repair in a murine calvarial critical bone defect model, likely through improved angiogenesis. In addition, *in vivo* MPM imaging provides a unique tool to understand angiogenesis and osteogenesis in bone scaffolds and enables further elucidation of whether a certain scaffold is beneficial to neovascularization. Intravital multiphoton microscopy imaging provides a modality for understanding the physiology and pathophysiology of angiogenesis in tissues and scaffolds. However, there are several limitations when using this technique. First, the surgical preparation requires particular expertise. Inflammation caused by unskilled operation will significantly decrease the MPM imaging quality. Second, due to the MPM imaging speed limitation, a custom-designed mouse head holder is needed to reduce the artifacts caused by heartbeat and respiration. Third, for long-term imaging, animals must be intraperitoneally or intravenously injected with saline to prevent dehydration.

## Disclosures

The authors declare that they have no competing financial interests.

## Acknowledgements

This study was supported by the Shenzhen Peacock Program, China (No. 110811003586331), the Shenzhen Basic Research Program (No. JCYJ20150401150223631, No. JCYJ20150401145529020, and No. JCYJ20160331190714896), the Guangdong Public Research and Capacity Building Special Program (No. 2015A020212030), the National Natural Science Foundation of China (No. 81501893), the National Major Basic Research Program of China (2013CB945503), and the SIAT Innovation Program for Excellent Young Researchers (Y5G010).

## References

1. Hu, X. *et al.* GPNMB enhances bone regeneration by promoting angiogenesis and osteogenesis: potential role for tissue engineering bone. *J Cell Biochem.* **114** (12), 2729-2737 (2013).
2. Schroeder, J. E., & Mosheiff, R. Tissue engineering approaches for bone repair: concepts and evidence. *Injury.* **42** (6), 609-613 (2011).
3. Chiarello, E. *et al.* Autograft, allograft and bone substitutes in reconstructive orthopedic surgery. *Aging Clin Exp Res.* **25 Suppl 1**, S101-103 (2013).
4. Elangovan, S. *et al.* The enhancement of bone regeneration by gene activated matrix encoding for platelet derived growth factor. *Biomaterials.* **35** (2), 737-747 (2014).
5. Bouyer, M. *et al.* Surface delivery of tunable doses of BMP-2 from an adaptable polymeric scaffold induces volumetric bone regeneration. *Biomaterials.* **104**, 168-181 (2016).
6. Rezwan, K. *et al.* Biodegradable and bioactive porous polymer/inorganic composite scaffolds for bone tissue engineering. *Biomaterials.* **27**(18), 3413-3431 (2006).
7. Burg, K. J., Porter, S., & Kellam, J. F. Biomaterial developments for bone tissue engineering. *Biomaterials.* **21**(23), 2347-2359 (2000).
8. Xiao, Y. *et al.* Modifications of collagen-based biomaterials with immobilized growth factors or peptides. *Methods.* **84**, 44-52 (2015).
9. Chen, G., & Lv, Y. Immobilization and Application of Electrospun Nanofiber Scaffold-based Growth Factor in Bone Tissue Engineering. *Curr Pharm Des.* **21** (15), 1967-1978 (2015).
10. Kofron, M. D., Li, X., & Laurencin, C. T. Protein- and gene-based tissue engineering in bone repair. *Curr Opin Biotechnol.* **15** (5), 399-405 (2004).
11. Chen, F. M. *et al.* New insights into and novel applications of release technology for periodontal reconstructive therapies. *J Control Release.* **149** (2), 92-110 (2011).
12. Winn, S. R. *et al.* Gene therapy approaches for modulating bone regeneration. *Adv Drug Deliv Rev.* **42** (1-2), 121-138 (2000).
13. Chang, P. C. *et al.* Adenovirus Encoding Human Platelet-Derived Growth Factor-B Delivered to Alveolar Bone Defects Exhibits Safety and Biodistribution Profiles Favorable for Clinical Use. *Hum Gene Ther.* **20** (5), 486-496 (2009).
14. Phipps, M. C., Xu, Y. Y., & Bellis, S. L. Delivery of Platelet-Derived Growth Factor as a Chemotactic Factor for Mesenchymal Stem Cells by Bone-Mimetic Electrospun Scaffolds. *Plos One.* **7** (7) (2012).
15. Gehmert, S. *et al.* Angiogenesis: The role of PDGF-BB on Adiopse-tissue derived Stem Cells (ASCs). *Clin Hemorheol and Microcirc.* **48**(1-3), 5-13 (2011).
16. Chang, P. C. *et al.* PDGF-B gene therapy accelerates bone engineering and oral implant osseointegration. *Gene Ther.* **17** (1), 95-104 gt2009117 [pii] (2010).
17. Javed, F. *et al.* Significance of the platelet-derived growth factor in periodontal tissue regeneration. *Arch Oral Biol.* **56** (12), 1476-1484 (2011).
18. Murali, R. *et al.* Biomimetic hybrid porous scaffolds immobilized with platelet derived growth factor-BB promote cellularization and vascularization in tissue engineering. *J Biomed Mater Res A.* **104** (2), 388-396 (2016).
19. Andrae, J., Gallini, R., & Betsholtz, C. Role of platelet-derived growth factors in physiology and medicine. *Genes Dev.* **22** (10), 1276-1312 (2008).
20. Wosnitza, M. *et al.* Plasticity of human adipose stem cells to perform adipogenic and endothelial differentiation. *Differentiation.* **75** (1), 12-23 (2007).
21. Hankenson, K. D. *et al.* Angiogenesis in bone regeneration. *Injury.* **42** (6), 556-561 (2011).
22. Schmidt, C. *et al.* Rapid three-dimensional quantification of VEGF-induced scaffold neovascularisation by microcomputed tomography. *Biomaterials.* **30** (30), 5959-5968 (2009).
23. Perng, C. K. *et al.* In Vivo Angiogenesis Effect of Porous Collagen Scaffold with Hyaluronic Acid Oligosaccharides. *J Surg Res.* **168** (1), 9-15 (2011).
24. Sun, Y. *et al.* Imaging tissue engineering scaffolds using multiphoton microscopy. *Microsc Res Tech.* **71** (2), 140-145 (2008).
25. Fan, X. *et al.* Noninvasive monitoring of placenta-specific transgene expression by bioluminescence imaging. *PLoS One.* **6** (1), e16348 (2011).
26. Yeo, M. G., & Kim, G. H. Preparation and Characterization of 3D Composite Scaffolds Based on Rapid-Prototyped PCL/beta-TCP Struts and Electrospun PCL Coated with Collagen and HA for Bone Regeneration. *Chem Mater.* **24** (5), 903-913 (2012).
27. Mao, Y. *et al.* Lentiviral Vectors Mediate Long-Term and High Efficiency Transgene Expression in HEK 293T cells. *Int J Med Sci.* **12** (5), 407-415 (2015).
28. Li, J. *et al.* Investigation of angiogenesis in bioactive 3-dimensional poly (D,L-lactide-co-glycolide)/nano-hydroxyapatite scaffolds by in vivo multiphoton microscopy in murine calvarial critical bone defect. *Acta Biomater.* **42**, 389-399 (2016).
29. Abbasi, H. *et al.* Lentiviral vector-mediated transduction of goat undifferentiated spermatogonia. *Anim Reprod Sci.* **163**, 10-17 (2015).
30. Pigossi, S. C. *et al.* Bacterial cellulose-hydroxyapatite composites with osteogenic growth peptide (OGP) or pentapeptide OGP on bone regeneration in critical-size calvarial defect model. *J Biomed Mater Res A.* (2015).
31. Bos, G. D. *et al.* The effect of histocompatibility matching on canine frozen bone allografts. *J Bone Joint Surg Am.*, **65** (1), 89-96 (1983).
32. Hollinger, J. O., & Kleinschmidt, J. C. The critical size defect as an experimental model to test bone repair materials. *J Craniofac Surg.* **1** (1), 60-68 (1990).
33. Hollanders, K. *et al.* Bevacizumab Revisited: Its Use in Different Mouse Models of Ocular Pathologies. *Curr Eye Res.* **40** (6), 611-621 (2015).
34. Gao, L. QSIM: quantitative structured illumination microscopy image processing in ImageJ. *Biomed Eng Online.* **14**, 4 (2015).
35. Kobat, D. *et al.* Deep tissue multiphoton microscopy using longer wavelength excitation. *Opt Express.* **17** (16), 13354-13364 (2009).

 

36. Lohmann, P. *et al.* Bone regeneration induced by a 3D architectured hydrogel in a rat critical-size calvarial defect. *Biomaterials.* **113**, 158-169 (2016).
37. Lv, J. *et al.* Enhanced angiogenesis and osteogenesis in critical bone defects by the controlled release of BMP-2 and VEGF: implantation of electron beam melting-fabricated porous Ti6Al4V scaffolds incorporating growth factor-doped fibrin glue. *Biomed Mater.* **10** (3) (2015).
38. Guldberg, R. E. *et al.* 3D imaging of tissue integration with porous biomaterials. *Biomaterials.* **29** (28), 3757-3761 (2008).
39. Boehler, R. M. *et al.* A PLG/HAp composite scaffold for lentivirus delivery. *Biomaterials.* **34** (21), 5431-5438 (2013).
40. Heo, S. J. *et al.* Fabrication and characterization of novel nano- and micro-HA/PCL composite scaffolds using a modified rapid prototyping process. *J Biomed Mater Res A.* **89** (1), 108-116 (2009).

 